Polymer Chemistry

ROYAL SOCIETY OF CHEMISTRY

PAPER

View Article Online
View Journal | View Issue

Cite this: *Polym. Chem.*, 2025, **16**, 3935

Bio-based poly(1,3-trimethyleneglycol-*co*-lactide) triblock copolymers: a promising platform for biomedical applications

Ernesto Tinajero Díaz, † Eduard Carles Zamora† and Antxon Martínez de Ilarduya *

A series of bio-based poly(lactide)-*b*-poly(1,3-trimethylene glycol)-*b*-poly(lactide) copolymers covering a wide range of compositions were synthesized by ring-opening polymerization (ROP) of L- or D,L-lactide initiated by bio-based poly(1,3-trimethylene glycol). The copolymers were obtained by bulk polymerizations carried out at 180 °C, using stannous octoate as the catalyst. The triblock structure was confirmed by both ^{1}H NMR and SEC analyses. It was observed that molecular weights increased while dispersities decreased with the increasing content of lactide units in the copolymer. Copolymers prepared with L-lactide exhibited crystallinity with melting points and enthalpies increasing with the length of lactide blocks in the copolymers. In contrast, copolymers based on *rac*-lactide were fully amorphous, regardless of composition. All copolymers exhibited a single glass transition temperature (T_g), which increased quasi-linearly with increasing lactide content, indicating good miscibility between polyether and polyester blocks. Furthermore, they demonstrated thermal stability up to approximately 250 °C and exhibited a two-step decomposition process, corresponding to the degradation of polyester and polyether segments. Finally, the amphiphilic nature of these copolymers was confirmed, as all of them were able to self-assemble in water, forming spherical nanoparticles with ζ-average diameters ranging from 95 to 158 nm.

Received 14th June 2025,
Accepted 28th July 2025

DOI: 10.1039/d5py00594a

rsc.li/polymers

Introduction

In the global transition to achieve a sustainable and circular economy, the introduction of innovative materials for packaging and biomedical applications from bioresource stocks is highly appreciated.[1–3] Poly(trimethylene glycol) (PO3G$_n$), for instance, is a fully bio-based polyether obtained by condensation of 1,3-propanediol (PDO), which is directly produced from a glucose fermentation proccess.[4,5] Interestingly, the chemical structure of PO3G$_n$ resembles that of poly(ethylene glycol) (PEG) with one additional methylene in the repeating unit. Typical molecular weights range from approximately 250 to 2700 g mol^{-1} and dispersities between 1.5 and 2.0.[6] Thus, the polyol can serve as a promising alternative to design novel polymer architectures. It has been used for the synthesis of renewable elastomeric thermoplastic polyesters,[7] polyamides[8] and polyurethanes.[6,9–12] On the other hand, in the biomedical field, the use of PEG in various pharmaceutical formulations, including cosmetics and soaps, among others, has been shown to induce the formation of anti-PEG antibodies, which can reduce the efficacy of PEGylated drugs.[13,14] Therefore, its replacement with PO3G$_n$ for different formulations could represent a promising alternative approach, although a lower degree of hydrophilicity can be expected. This polyol exhibits both lower critical solution temperature (LCST) and upper critical solution temperature (UCST) in the temperature range between 30 and 80 °C, and can be used for the preparation of thermosensitive nanomaterials.[5,15]

Poly(lactic acid) (PLA) is another interesting bio-based, biodegradable and biocompatible aliphatic polymer, obtained by ring-opening polymerization (ROP) of lactide (cyclic dimer of lactic acid).[16–18] The crystallinity of this polyester can be tuned through the enantiomeric composition of lactides used in the feed.[19,20] This polyester finds applications in the fields of packaging[21,22] and biomedicine.[16,23]

The integration of PO3G$_n$ and PLA presents a versatile platform for the development of fully biobased polymers with finely tunable properties. Owing to the presence of two terminal hydroxyl groups, PO3G$_n$ can act as an efficient macroinitiator for the ROP of lactide, leading to the formation of amphiphilic copolymers capable of self-assembling in aqueous environments.

This paper describes a protocol for the synthesis and characterization of poly(lactide-*b*-polytrimethylene glycol-*b*-lactide) tri-

Department d'Enginyeria Química, Universitat Politècnica de Catalunya, ETSEIB, Diagonal 647, 8028 Barcelona, Spain. E-mail: antxon.martinez.de.ilarduia@upc.edu
† These authors contributed equally.

block copolymers, abbreviated as PLA_m-*b*-$PO3G_n$-*b*-PLA_m, through bulk ROP of either L- or *rac*-lactide, covering a wide range of compositions. The polymerization was initiated by $PO3G_n$ macroinitiators of three different molecular weights ranging from 500 g mol^{-1} to 2400 g mol^{-1}. For each macroinitiator, three different triblock copolymers containing either L-lactide or *rac*-lactide were produced by varying the $PO3G_n$/lactide molar feed ratio. By precisely controlling the copolymer architecture, including composition, stereochemistry, and molecular weight, it was possible to modulate key material attributes such as thermal properties and stability. Finally, and as a proof-of-concept, we explored the ability of these copolymers to self-assemble in water using the emulsion/solvent-evaporation method. The biomedical field demands an expansion of available materials for drug delivery, especially for addressing challenges for an efficient delivery of therapeutic agents to the target site. $PO3G_n$, for example, can be an eco-friendly alternative to PEG, the gold-standard polymer used in drug delivery due to its 'stealth' properties; although already mentioned, it has proven to be less immunologically inert than originally anticipated.[24,25]

This strategy paves the way for the design of high-performance, sustainable materials tailored to meet the requirements of advanced technological and biomedical applications.

Experimental

Materials

Poly(trimethylene glycol) ($PO3G_n$, MW = 500 g mol^{-1}, 1000 g mol^{-1} and 2400 g mol^{-1}) was gifted by Allessa GmbH (Frankfurt, Germany). L/*rac*-Lactide (>99.0%) was donated by Corbion (Amsterdam, the Netherlands) and was stored in silica gel under vacuum at −10 °C prior to use. Tin-2-ethylhexanoate ($Sn(Oct)_2$ 92.5–100%) was acquired from Sigma-Aldrich and used as received. Poly(vinyl alcohol) (PVA, M_w = 3000 g mol^{-1}, 88% hydrolyzed) was obtained from Scientific Polymer Products. The solvents, chloroform ($CHCl_3$, ≥99.8%) and dichloromethane (DCM, ≥99.8%), were used as received.

General methods

^{1}H and ^{13}C NMR spectra were recorded on a Bruker AMX-300 spectrometer at 25 °C, operating at 300.1 and 75.5 MHz, respectively. Compounds were dissolved in deuterated chloroform ($CDCl_3$), and spectra were internally referenced to tetramethylsilane (TMS). About 10 and 50 mg of sample in 1 mL of solvent were used for ^{1}H and ^{13}C NMR analyses, respectively. Sixty-four scans were recorded for ^{1}H analysis, and between 5000 and 20 000 for ^{13}C NMR analysis.

Size exclusion chromatography (SEC). Molecular weights were determined using chloroform as the eluent in a Waters equipment (Foster City, CA, USA), equipped with RI and UV detectors and HR5E and HR2 Waters linear Styragel columns (7.8 mm × 300 mm). 0.1 mL (0.1% w/v) of the sample solution was injected and chromatographed at a flow rate of 0.5 mL min^{-1}. The molar mass averages and distributions were calibrated against PMMA standards.

Fourier transform infrared (FT-IR) spectra were acquired using a PerkinElmer Frontier FT-IR spectrometer (Waltham, MA, USA), equipped with a universal-attenuated total reflectance (ATR) accessory. Infrared spectra were recorded in the 4000–650 cm^{-1} range at a resolution of 4 cm^{-1}, and 16 scans were collected.

The thermal behaviour of polymers was examined by differential scanning calorimetry (DSC) using a PerkinElmer DSC 8000 apparatus. The thermograms were obtained from 4–6 mg samples at heating and cooling rates of 10 °C min^{-1} under a nitrogen flow of 20 mL min^{-1}. Indium and zinc were used as standards for temperature and enthalpy calibration. The glass transition temperature (T_g) was extracted from the inflection point of the heating traces recorded at 20 °C min^{-1} from melt-quenched samples, and the melting temperature was taken as the maximum of the endothermic peak in the heating traces recorded from samples crystallized from the melt.

Thermogravimetric analysis (TGA) was performed on a Mettler Toledo TGA/DSC 1 Star System under a nitrogen flow of 20 mL min^{-1} at a heating rate of 10 °C min^{-1} and within the temperature range of 30–600 °C.

Dynamic light scattering (DLS) measurements used for particle hydrodynamic size and ζ-potential determination were performed with a Malvern Nano ZS instrument equipped with a 4 mW He–Ne laser operated at 632.8 nm. Particles were suspended in deionized water at 25 °C and placed in glass cuvettes. The non-invasive back-scatter optic arrangement was used to collect the light scattered by particles at an angle of 173°.

Scanning electron microscopy (SEM) images were obtained with a field-emission JEOL JSM-7001F (JEOL, Tokyo, Japan) from platinum/palladium coated samples. Different dilutions were assayed to observe free individual nanoparticles. Images were edited using the ImageJ software.

Synthesis of PLA_m-$PO3G_n$-PLA_m triblock copolymers

Poly(L-lactide)$_m$-*b*-poly(trimethylene glycol)$_n$-*b*-poly(L-lactide)$_m$ ($PLLA_m$-*b*-$PO3G_n$-*b*-$PLLA_m$). As an example, for the synthesis of the $PLLA_{82}$-*b*-$PO3G_{41}$-*b*-$PLLA_{82}$ triblock copolymer with a [PO3G] : [L-LA] = [1] : [4] feed molar ratio, in a 25 mL three-neck, round-bottom flask equipped with a mechanical stirrer, a nitrogen inlet and a vacuum distillation outlet, $PO3G_{41}$ (MW = 2400, 0.5 g, 8.6 mmol of repeating units) and L-lactide (2.48 g, 17.2 mmol) were added. The flask was then immersed in an oil bath under a N_2 atmosphere for 5 min for purging the reaction system. Subsequently, the flask was heated to 120 °C and kept under vacuum for 5 additional min. Thereafter, the reaction flask was further heated to 180 °C, and polymerization began after the addition of $Sn(Oct)_2$ (1.2 mg, 3.06 μmol, 0.05% by weight relative to L-lactide) from a stock solution in chloroform. The reaction flask was left under stirring for ~1.5 h until L-lactide was fully consumed, as monitored by ^{1}H NMR spectroscopy. The mixture was then dissolved in DCM and precipitated into an excess of hexane. The copolymer was recovered as a white powder. Prior to characterization, the copolymer was dried at 50 °C under vacuum.

PLLA$_{82}$-*b*-PO3G$_{41}$-*b*-PLLA$_{82}$. ^{1}H NMR (300 MHz, $CDCl_3$, δ, ppm): 5.17 (q), 4.35 (q), 4.23 (m), 3.48 (t), 1.82 (qu), 1.58 (d). ^{13}C NMR (75.5 MHz, $CDCl_3$, δ, ppm): 169.5, 69.0, 67.8, 66.8, 30.1, 16.6.

PLLA$_m$-*b*-PO3G$_9$-*b*-PLLA$_m$ and PLLA$_m$-*b*-PO3G$_{17}$-*b*-PLLA$_m$ triblock copolymers. The synthesis of these copolymers was carried out in a similar fashion using the procedure described for the PLLA$_m$-*b*-PO3G$_{41}$-*b*-PLLA$_m$ copolymers using PO3G$_n$ macroinitiators having MW = 500 and 1000 g mol^{-1}, respectively.

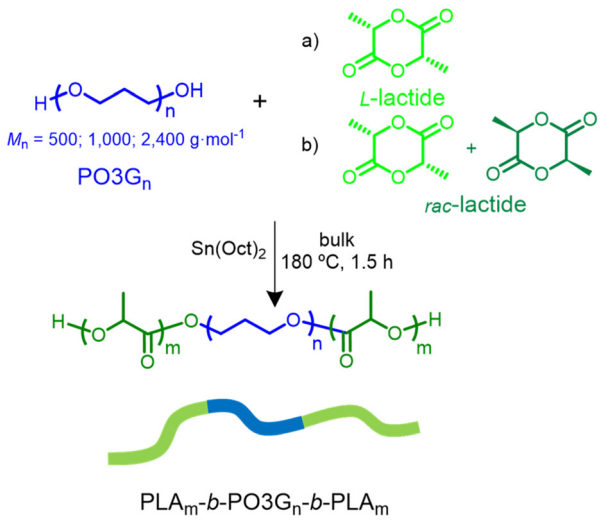

Scheme 1 Synthetic pathway for the preparation of bio-based poly (ether–ester)s triblock copolymers from PO3G$_n$ and (a) L-lactide or (b) *rac*-lactide.

Poly(*rac*-lactide)$_m$-*b*-poly(trimethylene glycol)$_n$-*b*-poly(*rac*-lactide)$_m$ (PrLA$_m$-*b*-PO3G$_n$-*b*-PrLA$_m$) copolymers were obtained using the same procedure, using *rac*-lactide (a 50 : 50 mixture of D- : L-lactide) instead of L-lactide and PO3G$_n$ macroinitiators having MW = 500, 1000 and 2400 g mol^{-1}.

Some copolymers were recovered either as a white powder or as a viscous oil, depending on the length of the macroinitiator used or the enantiomeric composition of the lactide used in the synthesis.

Preparation of nanoparticles

Nanoparticles were prepared using the oil-in-water single emulsion technique with minor modifications. Specifically, 10 mg of the PLA$_m$-*b*-PO3G$_n$-*b*-PLA$_m$ triblock copolymer was dissolved in 2 mL of DCM, and the solution was added to 10 mL of 1% (w/w) PVA aqueous solution. The mixture was sonicated using a Hielscher Ultrasonic Processor UP200St (E = 3200 J, c = 100, A = 20%) to yield a homogeneous oil-in-water emulsion. This emulsion was immediately poured into 10 mL of the 0.3% w/w PVA solution, and the mixture was magnetically stirred in an open beaker at room temperature for 3 h. The nanoparticles formed during the gradual evaporation of DCM. For SEM analysis, nanoparticles were collected by centrifugation at 9500 rpm for 15 min and washed three times with distilled water to remove the PVA emulsifier.

Results and discussion

The synthetic route for the synthesis of PLA$_m$-*b*-PO3G$_n$-*b*-PLA$_m$ triblock copolymers using Sn(Oct)$_2$ as a catalyst is shown in

Table 1 ROP of L/*rac*-lactide initiated by the PO3G$_n$ macroinitiator mediated by the Sn(Oct)$_2$ catalyst (0.05% w/w)

			Feed[b]	Experimental[c]		SEC		
Entry	Macroinitiator	Copolymer[a]	[PO3G$_n$]/[PLA]	[PO3G$_n$]/[PLA]	M_n (g mol^{-1})	M_n (g mol^{-1})	M_w (g mol^{-1})	$Đ$
1	PO3G$_9$				560	1030	1690	1.7
2		PLLA$_{4.5}$-*b*-PO3G$_9$-*b*-PLLA$_{4.5}$	50/50	56/44	1030	1680	2260	1.4
3		PLLA$_9$-*b*-PO3G$_9$-*b*-PLLA$_9$	33/67	38/62	1560	2540	3230	1.3
4		PLLA$_{18}$-*b*-PO3G$_9$-*b*-PLLA$_{18}$	20/80	22/78	2730	4630	5510	1.2
5		PrLA$_{4.5}$-*b*-PO3G$_9$-*b*-PrLA$_{4.5}$	50/50	57/43	920	1670	2230	1.3
6		PrLA$_9$-*b*-PO3G$_9$-*b*-PrLA$_9$	33/67	38/62	1650	2510	3130	1.3
7		PrLA$_{18}$-*b*-PO3G$_9$-*b*-PrLA$_{18}$	20/80	22/78	2930	4430	5380	1.2
8	PO3G$_{17}$				1140	1690	3530	2.1
9		PLLA$_{8.5}$-*b*-PO3G$_{17}$-*b*-PLLA$_{8.5}$	50/50	61/39	2050	2440	4360	1.8
10		PLLA$_{17}$-*b*-PO3G$_{17}$-*b*-PLLA$_{17}$	25/75	39/61	3900	5530	6805	1.2
11		PLLA$_{34}$-*b*-PO3G$_{17}$-*b*-PLLA$_{34}$	20/80	22/78	6030	10 010	11 770	1.2
12		PrLA$_{8.5}$-*b*-PO3G$_{17}$-*b*-PrLA$_{8.5}$	50/50	58/42	2290	3740	5280	1.4
13		PrLA$_{17}$-*b*-PO3G$_{17}$-*b*-PrLA$_{17}$	33/67	37/63	3830	5660	7120	1.3
14		PrLA$_{34}$-*b*-PO3G$_{17}$-*b*-PrLA$_{34}$	20/80	22/78	5230	7760	9510	1.2
15	PO3G$_{41}$				2510	4490	9270	2.1
16		PLLA$_{21}$-*b*-PO3G$_{41}$-*b*-PLLA$_{21}$	50/50	59/41	3920	7880	11 150	1.4
17		PLLA$_{41}$-*b*-PO3G$_{41}$-*b*-PLLA$_{41}$	33/67	43/57	5240	9230	12 410	1.3
18		PLLA$_{82}$-*b*-PO3G$_{41}$-*b*-PLLA$_{82}$	20/80	23/77	11 710	19 030	23 080	1.2
19		PrLA$_{21}$-*b*-PO3G$_{41}$-*b*-PrLA$_{21}$	50/50	61/39	3850	6830	10 250	1.5
20		PrLA$_{41}$-*b*-PO3G$_{41}$-*b*-PrLA$_{41}$	33/67	45/55	5070	7760	11 050	1.4
21		PrLA$_{82}$-*b*-PO3G$_{41}$-*b*-PrLA$_{82}$	20/80	22/78	13 830	16 730	21 600	1.3

[a] Subscripts correspond to the degree of polymerization (DP) of each block used in the feed. [b] Molar feed ratio of PO3G$_n$ and PLA repeating units. [c] Experimental composition and M_n, calculated from OCH/OCH$_2$ signals and end groups analysis, respectively, by ^{1}H NMR spectroscopy.

Scheme 1. Three types of PO3G$_n$ macroinitiators differing in the molecular weight were used. For each macroinitiator, three series of triblock copolymers containing L- or *rac*-lactide were obtained by varying the PO3G$_n$/lactide ratios. The results of these syntheses including molar feed ratios, compositions and molecular weights for the whole library of copolymers are provided in Table 1. The PO3G$_n$ macroinitiator exhibits two hydroxyl-end groups, which can trigger the ROP of cyclic esters, *e.g.*, L/*rac*-lactide, when assisted by a suitable catalyst.

We selected Sn(Oct)$_2$ because this catalyst is approved by the FDA for use in food and medical applications and has high activity in the synthesis of PLA.[17] The reaction took place in bulk at 180 °C and was easily followed by ^{1}H NMR analysis as the methine signals from the lactide monomer (CH, 5.03 ppm) and polymer (CH, 5.17 ppm) appeared well-resolved (Fig. 1a and Fig. S1 of the SI). By comparing both signals, it is possible to quantify the unreacted monomer. We first explored the evolution of the ROP of L-lactide initiated by PO3G$_{41}$ (M_n = 2400 g mol^{-1}) (Fig. 1b). A burst in the early stage of the ROP is observed, with 91% of L-lactide reacting after 30 min. Subsequently, the polymerization proceeded steadily until equilibrium was reached and approximately 96% of the monomer was consumed in nearly 1.5 h. Three different concentrations of the Sn(Oct)$_2$ catalyst were tested, and based on both the conversion over time results and the catalyst amount (Fig. 1b), the intermediate concentration (0.05% by weight of lactide) was ultimately selected. The ROP of L-lactide proceeded satisfactorily in a relatively short time; nonetheless, species other than the selected macroinitiator, *i.e.*, water, can indeed interfere in the polymerization and parallelly compete for a site in the final polymer architecture. As we will show later, this side reaction was not observed during the synthesis of these copolymers, as the ratio of reacted macroinitiator end groups to triblock copolymer end groups was close to one.

After purification, we took samples of the PO3G$_n$ macroinitiator and the block copolymers to determine the molecular weight distributions (MWDs) by SEC analysis. Table 1 shows the SEC data for the macroinitiators and triblock copolymers. As expected, triblock copolymers exhibited higher molecular weights than their respective macroinitiators, which increased with the content of lactide in the copolymers. The dispersity ($Đ$) of the PO3G$_n$ macroinitiators ranged from 1.7 to 2.1. On the other hand, in all series, $Đ$ was observed to decrease as the molecular weight or the content of lactide units in the copolymer increased. $Đ$ values of 1.2–1.3 were obtained for the copolymers with a higher content of lactide. Monomodal and narrow MWDs were obtained, indicating excellent control over the polymerization (Fig. 2). The results suggest that Sn(Oct)$_2$ serves as an efficient catalyst for the ROP of lactide, initiated by the macroinitiator, with significantly reduced interchain transesterification. Thus, SEC traces provided evidence that the –OH end groups in PO3G$_n$ were the sole species that initiated the ROP of lactide. The constitution and composition of the copoly(ether–ester)s were ascertained by ^{1}H and ^{13}C NMR spectroscopy, which clearly discriminates between methylene and methine protons from PO3G$_n$ and L-lactide

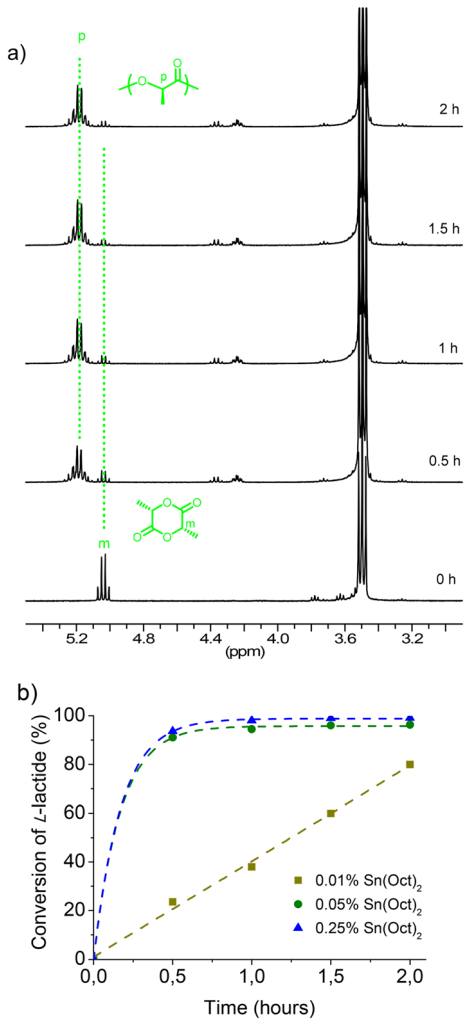

Fig. 1 (a) ^{1}H-NMR ($CDCl_3$) spectra of the PLLA$_{21}$-*b*-PO3G$_{41}$-*b*-PLLA$_{21}$ copolymer at different reaction times using 0.05% Sn(Oct)$_2$ catalyst and (b) conversion of L-lactide in the ROP initiated by the PO3G$_{41}$ macroinitiator at different catalyst concentrations.

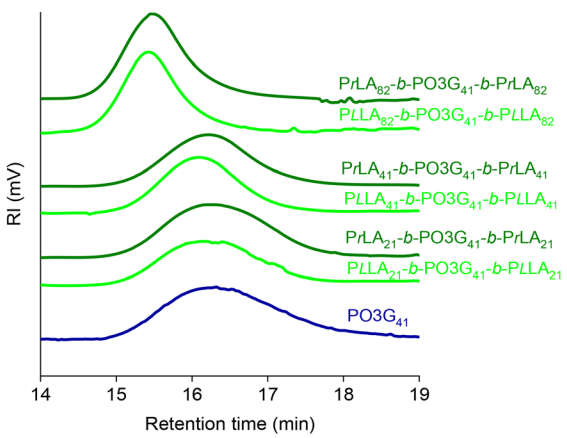

Fig. 2 SEC traces of the PO3G$_{41}$ macroinitiator and the PLA$_m$-*b*-PO3G$_{41}$-*b*-PLA$_m$ triblock copolymers.

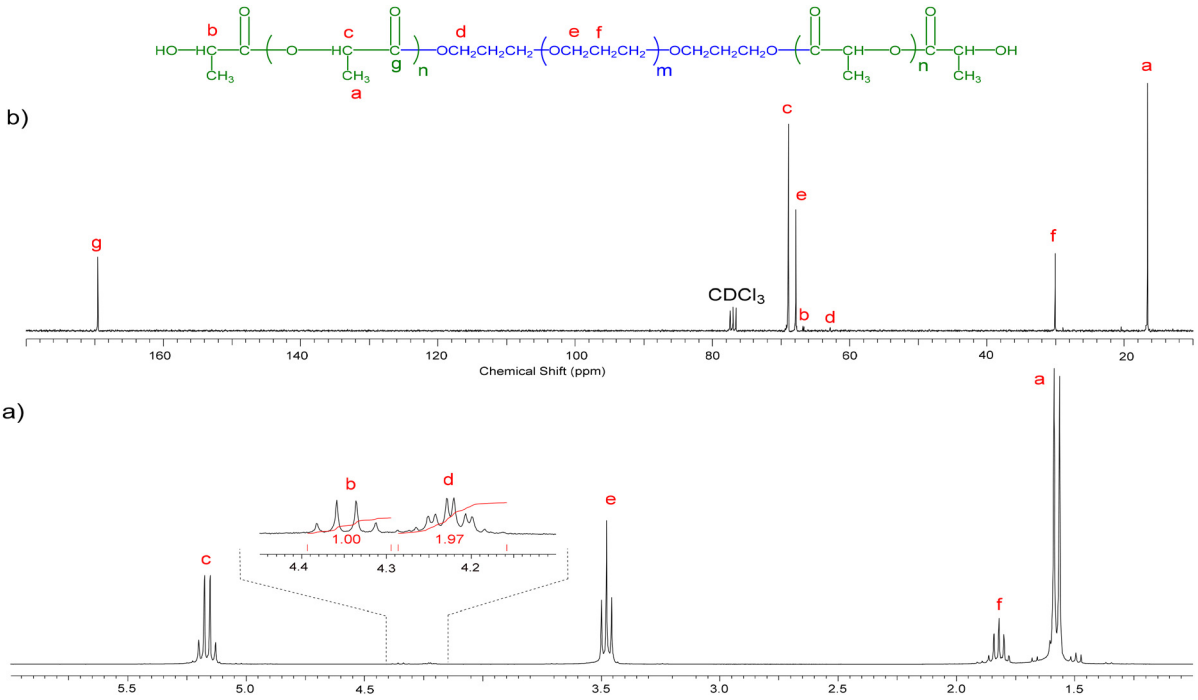

Fig. 3 (a) ^{1}H- and (b) ^{13}C-NMR spectra in $CDCl_3$ of the $PLLA_{82}$-*b*-$PO3G_{41}$-$PLLA_{82}$ copolymer.

units, respectively. As an example, Fig. 3 shows the representative NMR spectra recorded for the $PLLA_{82}$-*b*-$PO3G_{41}$-*b*-$PLLA_{82}$ copolymer. Compositions were determined by integration of the CH signal of lactide units (signal c) and the first methylene protons of $PO3G_n$ units (signal e). The composition for all series was close to that of $PO3G_n$ and L-lactide used in the feed and exhibited acceptable consistency, with small deviations due to partial volatilization of lactide during ROP. On the other hand, the signal corresponding to the methylene protons of $PO3G_n$ attached to the first lactide unit (signal d), which appeared as a multiplet, showed an integral twice that of the C*H*OH end groups (signal b). This further confirmed the triblock structure of the copolymers and the absence of any PLA chains initiated by other species, such as water. Spectra recorded for $PrLA_{82}$-*b*-$PO3G_{41}$-*b*-$PrLA_{82}$ and two selected $PLLA_m$-*b*-$PO3G_{41}$-*b*-$PLLA_m$ and $PrLA_m$-*b*-$PO3G_{41}$-*b*-$PrLA_m$ series can be found in Fig. S2–S6 of the SI. The spectra of triblock copolymers obtained using *rac*-lactide instead of L-lactide showed broader signals in the ^{1}H NMR spectra and splitting in the ^{13}C NMR peaks due to the presence of different stereosequences in the PLA blocks (Fig. S2).[26]

In addition, FT-IR further corroborated the chemical structure of the obtained copolymers (Fig. 4). The infrared spectrum of $PO3G_{41}$ exhibited a strong absorption band at 1102 cm^{-1}, corresponding to the C–O–C asymmetric stretching vibration of the ether groups. The incorporation of lactide units at the end groups of $PO3G_n$ to form the triblock copolymer was confirmed by the presence of the C═O carbonyl band at 1751 cm^{-1} and the C(═O)–O stretching band at 1181 cm^{-1}, which are characteristics of the ester groups of the lactide units. These absorptions increased in intensity as the lactide content increased in the $PLLA_m$-*b*-$PO3G_{41}$-*b*-$PLLA_m$ copolymer series. Furthermore, signals attributed to CH_2 stretching (2859 cm^{-1}) decreased, while those related to CH_3 bending (1453 cm^{-1}) increased, as the copolymer was enriched in lactide units.

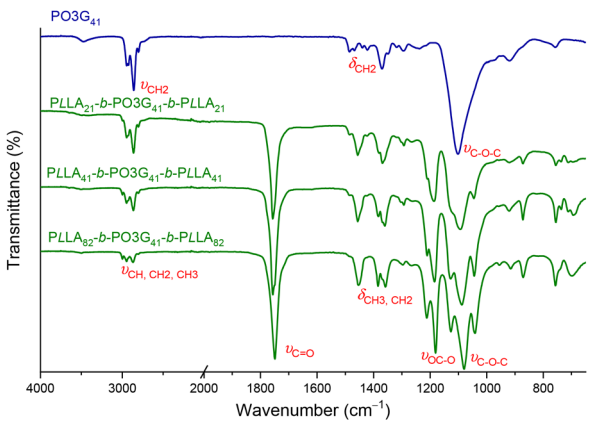

Fig. 4 FT-IR spectra of the $PO3G_{41}$ macroinitiator and $PLLA_m$-*b*-$PO3G_{41}$-*b*-$PLLA_m$ triblock copolymers.

Thermal properties of triblock copolymers

To investigate the thermal stability and transitions of these copolymers, TGA and DSC analyses were performed. The data collected using these analyses for each series of PLA_m-*b*-$PO3G_n$-*b*-PLA_m triblock copolymers, as well as for the $PO3G_n$ macroinitiators, are given in Table 2. The TGA traces recorded for the PLA_m-

Table 2 Thermal properties of the PLA_m-*b*-$PO3G_n$-*b*-PLA_m triblock copolymers

	TGA[a]				DSC[b]						
					Cooling			Second heating			
Polymer	$^{\circ}T_d$ (°C)	$^{max}T_d$ (°C)	R_w (%)	[PO3G]/[PLA]	T_g (°C)	T_c (°C)	ΔH_c (J g^{-1})	T_{cc} (°C)	ΔH_{cc} (J g^{-1})	T_m (°C)	ΔH_m (J g^{-1})
$PO3G_9$	248	398	0	100/0	−82	—	—	−40	−60	10	70
$PLLA_{4.5}$-*b*-$PO3G_9$-*b*-$PLLA_{4.5}$	247	282/410	1	42/58	−41	—	—	—	—	—	—
$PLLA_9$-*b*-$PO3G_9$-*b*-$PLLA_9$	250	281/408	0	25/75	−11	—	—	—	—	—	—
$PLLA_{18}$-*b*-$PO3G_9$-*b*-$PLLA_{18}$	246	273/391	1	13/87	15	—	—	80	−9	107	13
$PrLA_{4.5}$-*b*-$PO3G_9$-*b*-$PrLA_{4.5}$	261	282/404	1	45/55	−43	—	—	—	—	—	—
$PrLA_9$-*b*-$PO3G_9$-*b*-$PrLA_9$	273	301/401	1	25/75	−17	—	—	—	—	—	—
$PrLA_{18}$-*b*-$PO3G_9$-*b*-$PrLA_{18}$	260	289/395	1	14/86	8	—	—	—	—	—	—
$PO3G_{17}$	335	410	1	100/0	−77	—	—	−40	−64	13	93
$PLLA_{8.5}$-*b*-$PO3G_{17}$-*b*-$PLLA_{8.5}$	246	269/425	1	49/51	−44	—	—	—	—	—	—
$PLLA_{17}$-*b*-$PO3G_{17}$-*b*-$PLLA_{17}$	238	286/417	0	32/68	−6	—	—	33/68	−11/−15	100	15
$PLLA_{34}$-*b*-$PO3G_{17}$-*b*-$PLLA_{34}$	247	270/411	0	18/82	26	94	−36	—	—	144	38
$PrLA_{8.5}$-*b*-$PO3G_{17}$-*b*-$PrLA_{8.5}$	242	266/424	1	49/51	−41	—	—	—	—	—	—
$PrLA_{17}$-*b*-$PO3G_{17}$-*b*-$PrLA_{17}$	246	268/407	2	31/69	−13	—	—	—	—	—	—
$PrLA_{34}$-*b*-$PO3G_{17}$-*b*-$PrLA_{34}$	246	268/407	1	19/81	12	—	—	—	—	—	—
$PO3G_{41}$	306	381	0	100/0	−75	—	—	−40	−57	17	80
$PLLA_{21}$-*b*-$PO3G_{41}$-*b*-$PLLA_{21}$	261	273/428	0	51/49	−33	57/23	−7/−2	65	−3	100	4
$PLLA_{41}$-*b*-$PO3G_{41}$-*b*-$PLLA_{41}$	272	289/428	0	37/63	−14	77	−26	—	—	126	26
$PLLA_{82}$-*b*-$PO3G_{41}$-*b*-$PLLA_{82}$	252	275/408	0	18/82	32	95	−36	—	—	156	41
$PrLA_{21}$-*b*-$PO3G_{41}$-*b*-$PrLA_{21}$	241	254/428	0	54/46	−49	—	—	—	—	—	—
$PrLA_{41}$-*b*-$PO3G_{41}$-*b*-$PrLA_{41}$	251	286/408	1	38/62	−16	—	—	—	—	—	—
$PrLA_{82}$-*b*-$PO3G_{41}$-*b*-$PrLA_{82}$	260	315/412	1	18/82	26	—	—	—	—	—	—
$PLLA_{68}$	255	338	0	100/0	47	101	−40	88	−10	152	47
$PrLA_{68}$	287	354	0	100/0	43	—	—	—	—	—	—

[a] Onset temperature for 10% weight loss ($^{\circ}T_d$), maximum decomposition rate temperature ($^{max}T_d$), remaining weight (R_w) and weight% composition ([PO3G]/[PLA]) after heating at 600 °C. [b] Glass transition (T_g), crystallization (T_c and ΔH_c) and melting (T_m and ΔH_m) temperatures and enthalpies measured by DSC.

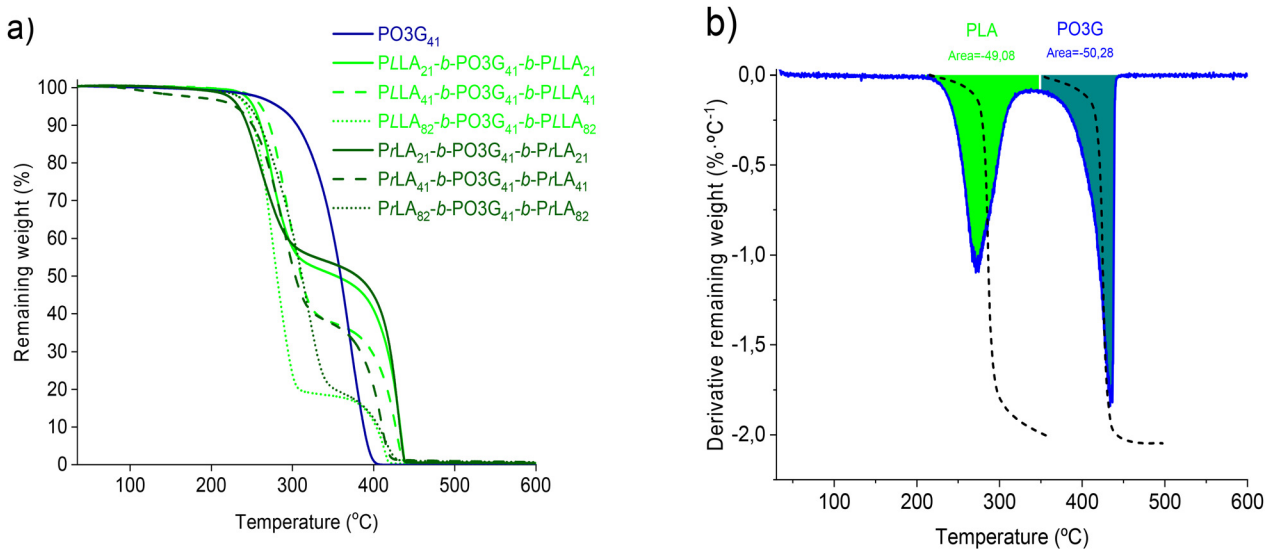

Fig. 5 (a) TGA traces of the $PO3G_{41}$ and PLA_m-*b*-$PO3G_{41}$-*b*-PLA_m copolymers and (b) the derivative curve of the $PLLA_{21}$-*b*-$PO3G_{41}$-*b*-$PLLA_{21}$ copolymer.

b-$PO3G_{41}$-*b*-PLA_m series and their derivative curves are shown in Fig. 5. For the rest of the series, both TGA traces and derivative curves are provided in Fig. S7 and S8 of the SI. The onset temperature ($^{\circ}T_d$) of $PO3G_{41}$ decreased in the copolymers as polylactide blocks were incorporated at its ends; in contrast, the derivative curve split into two main events: the maximum decomposition rate ($^{max}T_d$) exhibited two maxima at temperatures close to those of their parent polymers: the former found in the 273–289 °C range, which was ascribed to the degradation of PLA blocks, and the latter ranging from 408 to 428 °C, attributed to the degradation of the more thermally stable $PO3G_{41}$ block. It is noteworthy to highlight that there was no more than 1% residue left at temperatures far from 450 °C, and in several cases, there was no residue at all.

Minor differences in the thermal analysis were observed for the PLA_m-*b*-$PO3G_9$-*b*-PLA_m and PLA_m-*b*-$PO3G_{17}$-*b*-PLA_m series, with deviations hardly surpassing 10% in some cases (Fig. S7 and S8 of the SI). The TGA, additionally, provided valuable information on the chemical constitution. Since the derivative curve exhibited two well-defined and resolved decomposition steps, the composition of each copolymer could be ascertained by integration of these curves. Fig. 5b, for instance, shows the derivative curve of the $PLLA_{21}$-*b*-$PO3G_{41}$-*b*-$PLLA_{21}$ copolymer: the areas under each curve reveal direct composition by weight of the copolymers. The extracted values for each series (Table 2) are close, with small variations compared to those obtained by ^{1}H NMR spectroscopy (Table 1). To explore the influence of copolymer composition on crystallinity and

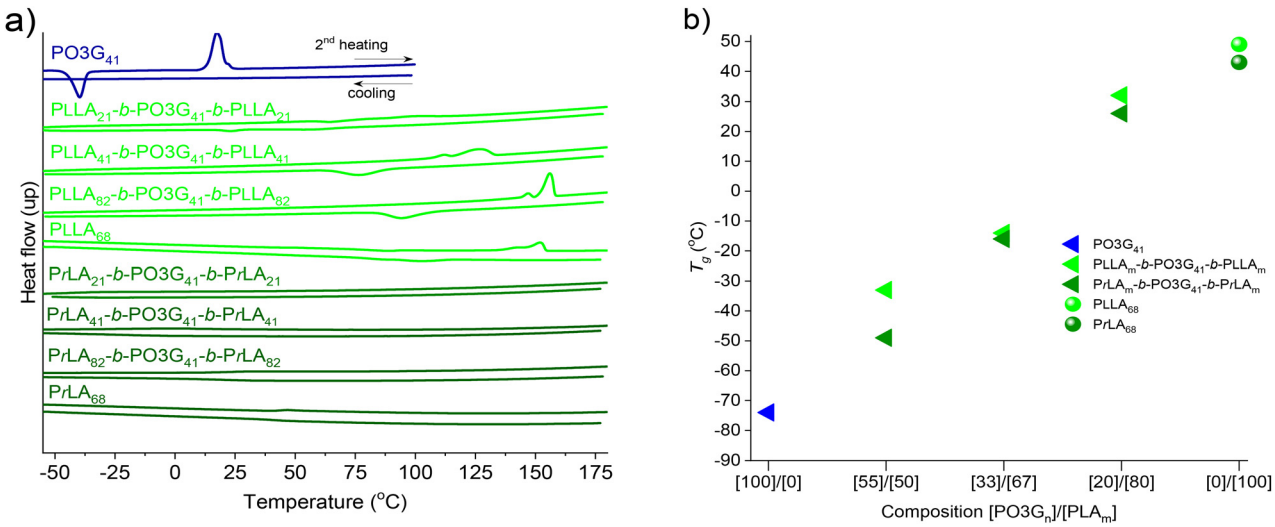

Fig. 6 (a) DSC second heating and cooling traces of the PLA_m-*b*-$PO3G_{41}$-*b*-PLA_m triblock copolymers and (b) T_g *vs.* molar composition of PLA_m-*b*-$PO3G_{41}$-*b*-PLA_m copolymers.

melting temperatures, DSC was used to investigate their thermal behavior. In Fig. 6a, we present a comparative view of the recorded DSC traces from cooling scans and second heating for the PLLA$_m$-*b*-PO3G$_{41}$-*b*-PLLA$_m$ and P*r*LA$_m$-*b*-PO3G$_{41}$-*b*-P*r*LA$_m$ copolymer series as well as their parent macroinitiator. PO3G$_{41}$ exhibits an endothermic peak at 17 °C due to the melting process of the macroinitiator crystalline domains after a cold crystallization process that was observed to happen at −40 °C. For all copolymer series, no peak due to melting or crystallization of the inner macroinitiator was observed. This phenomenon can be attributed to the PLA segments attached to the PO3G$_n$ end groups that restrict the chain mobility.[27,28] On the other hand, there was a clear trend in the melting process attributed to the PLA segments, situated in the 95–155 °C range. As the composition or the length of the L-lactide blocks in the copolymers increases, the melting temperature shifts to the value observed for its parent homopolymer, *i.e.*, PLLA$_{68}$. This shift toward higher temperatures, approaching the melting point of PLLA, is directly correlated with the degree of polymerization (DP) of the lactide blocks. In other words, as the DP of the PLA segments increases, the melting temperature of the copolymers also rises. This behavior can be attributed to an increase in lamellar thickness, as longer chains are capable of forming more stable and thicker crystalline lamellae. When the copolymers are cooled from the melt, a crystallization event appears and follows a similar trend to the copolymer composition changes. As it was expected, P*r*LA$_m$-*b*-PO3G$_{41}$-*b*-P*r*LA$_m$ copolymers did not exhibit any (*endo*/*exo*) thermic peak. Similar behavior was observed for the PLA$_m$-*b*-PO3G$_{9/34}$-*b*-PLA$_m$ copolymers, whose thermograms are provided in Fig. S9–S11 of the SI.

All of the copolymers exhibited a single, second-order glass transition temperature (T_g), which increased almost linearly with the lactide content in all the series of copolymers studied. Fig. 6b shows the plot of T_g *versus* composition for the PLA$_m$-*b*-PO3G$_{41}$-*b*-PLA$_m$ series. As illustrated, the copolymer T_g values fall between −49 °C and 32 °C, intermediate to those of PO3G$_{41}$ and PLA$_{68}$ homopolymers (Fig. S12), confirming the full miscibility between the PLA and PO3G$_n$ blocks.[10,29]

Table 3 *Z*-Average diameter (nm), PDI and zeta potential (ζ) of the nanoparticles obtained from PLA$_m$-*b*-PO3G$_{41}$-*b*-PLA$_m$ triblock copolymers

Copolymer	Size (nm)	PDI	ζ (mV)
PLLA$_{21}$-*b*-PO3G$_{41}$-*b*-PLLA$_{21}$	171	0.09	−5
PLLA$_{41}$-*b*-PO3G$_{41}$-*b*-PLLA$_{41}$	170	0.08	−9
PLLA$_{82}$-*b*-PO3G$_{41}$-*b*-PLLA$_{82}$	124	0.12	−4
P*r*LA$_{21}$-*b*-PO3G$_{41}$-*b*-P*r*LA$_{21}$	104	0.17	−10
P*r*LA$_{41}$-*b*-PO3G$_{41}$-*b*-P*r*LA$_{41}$	95	0.24	−8
P*r*LA$_{82}$-*b*-PO3G$_{41}$-*b*-P*r*LA$_{82}$	109	0.13	−9

Self-assembling in aqueous media

In the search for innovative nanomaterials, we explored the ability of the PLA$_m$-*b*-PO3G$_n$-*b*-PLA$_m$ amphiphilic triblock copolymers to self-assemble in water. We used the well-established emulsion-evaporation method for obtaining the nanoparticles due to the good solubility of copolymers in DCM,[30,31] enabling the fabrication of a library of nanomaterials. As representative

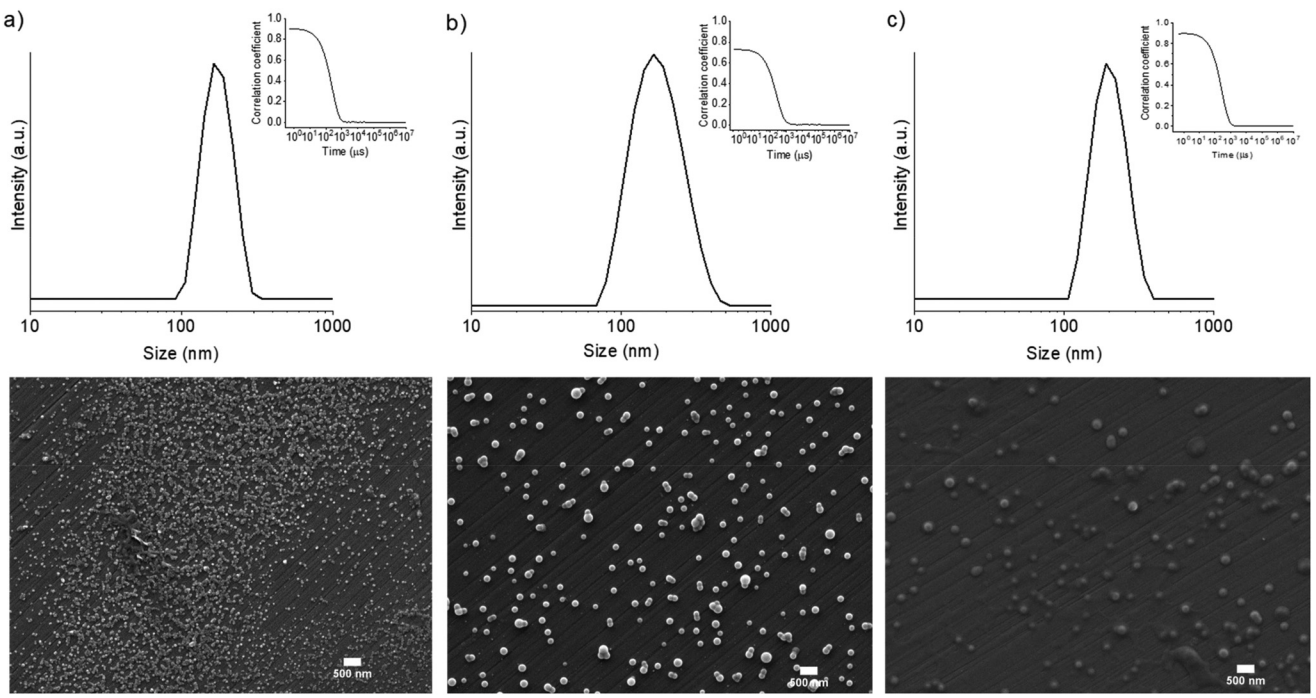

Fig. 7 (Top) DLS profiles (inset: correlation coefficient) and (bottom) SEM images of (a) P*r*LA$_{82}$-*b*-PO3G$_{41}$-*b*-P*r*LA$_{82}$, (b) P*r*LA$_{41}$-*b*-PO3G$_{41}$-*b*-P*r*LA$_{41}$ and (c) PLLA$_{21}$-*b*-PO3G$_{41}$-*b*-PLLA$_{21}$ triblock copolymers. Scale bar = 500 nm.

examples, Table 3 provides sizes, polydispersity indexes (PDI's) and zeta potentials (ζ) acquired by DLS measurements for the PLA$_m$-*b*-PO3G$_{41}$-*b*-PLA$_m$ copolymer series. Unimodal distributions evidenced the occurrence of a self-assembling event, while *Z*-average diameters oscillating between 95 and 171 nm and narrow PDIs confirmed the presence of nanometric aggregates (Fig. 7a–c). The correlation coefficients, whose values were close to 1 (inset in DLS profiles), strengthened the reliability and quality of the DLS data. Interestingly, NPs from P*r*LA$_m$-*b*-PO3G$_{41}$-*b*-P*r*LA$_m$ copolymers exhibited smaller sizes than PLLA$_m$-*b*-PO3G$_{41}$-*b*-PLLAm, a fact that could be a direct consequence of the amorphous or semicrystalline structure adopted by the hydrophobic core in the nanoparticle. The amorphous PLA blocks can pack more efficiently than semicrystalline blocks in the core of the nanoparticles, allowing the nanoparticles to self-assemble with reduced dimensions.[32] DSC scans of two types of selected nanoparticles revealed two key observations (Fig. S13 of the SI). First, the T_g values of the self-assembled copolymers were found to be 23 and 26 °C higher than those of the corresponding bulk materials. This suggests that during the self-assembly process, the PLA and PO$_3$G$_n$ blocks rearrange according to their affinity for water, forming a core–shell nanostructure with well-defined nanoscale phase segregation. Second, the T_g of nanoparticles derived from *rac*-lactide showed enthalpic relaxation phenomena, indicating efficient packing and compaction of the amorphous chains. In all cases, nanoparticles exhibited negative zeta potentials, with values hardly different across the entire series. DLS data for the PLA$_m$-*b*-PO3G$_{9/17}$-*b*-PLA$_m$ series can be found in Table S1 of the SI. *Z*-Average diameters between 102 and 158 nm and negative *z*-potentials ranging from −4 to −20 were obtained for the PLA$_m$-*b*-PO3G$_9$-*b*-PLA$_m$ copolymers. The PLA$_m$-*b*-PO3G$_{17}$-*b*-PLA$_m$ exhibited *z*-average diameters of 115–144 nm with negative *z*-potentials in the −2 to −20 range. To further comprehend the adopted morphology of these nanoaggregates, SEM shed light on their shape. Illustrative images from selected copolymers are shown in Fig. 7, bottom. To our delight, we observed well-delineated spherical nanoobjects, whose sizes matched with those obtained by DLS.

Conclusions

A bio-based polyol derived from 1,3-propanediol was employed to prepare triblock copoly(ether–ester)s. The two hydroxyl end groups of the PO3G$_n$ polyol serve as efficient initiators for the ROP of L-lactide or *rac*-lactide. Using solventless ROP, we generated a library of BAB-type copolymers with predictable degrees of polymerization, whose compositions were readily tuned by varying the [PO3G]/[lactide] feed ratio. Thermal analysis showed these copolymers to be stable up to approximately 250 °C, undergoing decomposition in a two-step process. Crystallinity could be adjusted by selecting the lactide stereochemistry and tailoring the triblock composition. Since PLA and PO3G$_n$ segments are fully miscible, the glass transition temperature (T_g) of the entire series can be modulated simply by altering the [PO3G]/[lactide] ratio, enabling precise control over material properties. These novel, fully bio-based polymers exhibit pseudo-amphiphilic behaviour in aqueous solution. As a proof-of-concept, dynamic light scattering (DLS) and scanning electron microscopy (SEM) confirmed that the poly(ether–ester) copolymers self-assembled into nanometric particles in water. We anticipate that this protocol will pave the way for designing innovative nanodevices that could be used for biomedical applications *via* ROP of different cyclic esters using PO3G$_n$ as a macroinitiator.

Author contributions

A. M. de I. conceived the idea and proposed the strategy. E. T. D., E. C. Z. and A. M. de I. designed the experiments, carried out the experimental work, evaluated the data, and wrote the manuscript together. All participated in data analysis. All the authors proofread the manuscript.

Conflicts of interest

There are no conflicts to declare.

Data availability

All data supporting the findings of this study are available within the article and its SI. Raw experimental data are available from the corresponding author upon reasonable request.

^{1}H-NMR ($CDCl_3$) spectra of P*LLA*$_{21}$-*b*-PO3G$_{41}$-*b*-P*LLA*$_{21}$ copolymer at different reaction times using a) 0.01% and b) 0.25% Sn(Oct)$_2$ catalyst concentration. ^{1}H and ^{13}C NMR spectra ($CDCl_3$) of the P*r*LA$_{82}$-*b*-PO3G$_{41}$-*b*-P*r*LA$_{82}$ copolymer. ^{1}H-NMR ($CDCl_3$) of the P*LLA*$_m$-*b*-PO3G$_{41}$-*b*-P*LLA*$_m$. ^{13}C-NMR ($CDCl_3$) of the P*LLA*$_m$-*b*-PO3G$_{41}$-*b*-P*LLA*$_m$. ^{1}H-NMR ($CDCl_3$) of the P*r*LA$_m$-*b*-PO3G$_{41}$-*b*-P*r*LA$_m$. ^{13}C-NMR ($CDCl_3$) of the P*r*LA$_m$-*b*-PO3G$_{41}$-*b*-P*r*LA$_m$. TGA traces and derivatives curves of the PLA$_m$-*b*-PO3G$_9$-*b*-PLA$_m$ triblock copolymers.TGA traces and derivatives curves of the PLA$_m$-*b*-PO3G$_{17}$-*b*-PLA$_m$ triblock copolymers. Second heating and cooling and third heating and cooling DSC traces of the PLA$_m$-*b*-PO3G$_9$-*b*-PLA$_m$ triblock copolymers. Second heating and cooling and third heating and cooling DSC traces of the PLA$_m$-*b*-PO3G$_{17}$-*b*-PLA$_m$ triblock copolymers. DSC third heating traces of the PLA$_m$-*b*-PO3G$_{41}$-*b*-PLA$_m$ triblock copolymers. DSC third heating of PO3G$_n$ and PLA$_{68}$ homopolymers. DSC traces of P*LLA*$_{82}$-b-PO3G$_{41}$-b-P*LLA*$_{82}$ and P*r*LA$_{82}$-b-PO3G$_{41}$-b-P*r*LA$_{82}$ copolymers in bulk and self-assembled nanoparticles. Table with *Z*-average diameters (nm), PDI and zeta potential (**z**) of PLA$_m$-*b*-PO3G$_n$-*b*-PLA$_m$ triblock copolymers. See DOI: **https://doi.org/10.1039/d5py00594a**

Acknowledgements

The authors would like to thank the Ministerio de Ciencia, Innovación y Universidades of Spain (MCIU/AEI/FEDER, UE)

(project RTI2018-095041-B-C33) and the Technological University of Catalonia (UPC) (AGRUPS R-02520) for their financial support. The authors would also like to acknowledge Dr Judit Canadell (TotalEnergies-Corbion) for the L- and *rac*-lactide monomers and Dr Peter Talbiersky from Allessa for kindly providing the $PO3G_n$ samples for this study. E. T. D. acknowledges the postdoctoral grant Margarita Salas awarded in 2021 by the Spanish Government.

References

1 J.-G. Rosenboom, R. Langer and G. Traverso, Bioplastics for a circular economy, *Nat. Rev. Mater.*, 2022, **7**(2), 117–137, DOI: **10.1038/s41578-021-00407-8**.

2 B. von Vacano, H. Mangold, G. W. M. Vandermeulen, G. Battagliarin, M. Hofmann, J. Bean and A. Künkel, Sustainable Design of Structural and Functional Polymers for a Circular Economy, *Angew. Chem., Int. Ed.*, 2023, **62**(12), e202210823, DOI: **10.1002/anie.202210823**.

3 H. Sardon, D. Mecerreyes, A. Basterretxea, L. Avérous and C. Jehanno, From Lab to Market: Current Strategies for the Production of Biobased Polyols, *ACS Sustainable Chem. Eng.*, 2021, **9**(32), 10664–10677, DOI: **10.1021/acssuschemeng.1c02361**.

4 M. A. Harmer, D. C. Confer, C. K. Hoffman, S. C. Jackson, A. Y. Liauw, A. R. Minter, E. R. Murphy, R. E. Spence and H. B. Sunkara, Renewably sourced polytrimethylene ether glycol by superacid catalyzed condensation of 1,3-propanediol, *Green Chem.*, 2010, **12**(8), 1410–1416, DOI: **10.1039/c002443k**.

5 H.-N. Lee, B. M. Rosen, G. Fenyvesi and H. B. Sunkara, UCST and LCST phase behavior of poly(trimethylene ether) glycol in water, *J. Polym. Sci., Part A: Polym. Chem.*, 2012, **50**(20), 4311–4315, DOI: **10.1002/pola.26242**.

6 A. Delavarde, G. Savin, P. Derkenne, M. Boursier, R. Morales-Cerrada, B. Nottelet, J. Pinaud and S. Caillol, Sustainable polyurethanes: toward new cutting-edge opportunities, *Prog. Polym. Sci.*, 2024, **151**, 101805, DOI: **10.1016/j.progpolymsci.2024.101805**.

7 Y. Li, Y. Liu, A. Liu, C. Xu, C. Zhang, J. Yu, R. Yuan and F. Li, Poly(trimethylene terephthalate-b-poly(trimethylene ether) glycol) copolymers: From bio-based thermoplastic elastomers to elastic fibers for apparel, *Eur. Polym. J.*, 2025, **225**, 113706, DOI: **10.1016/j.eurpolymj.2024.113706**.

8 J. Jiang, Q. Tang, X. Pan, Z. Xi, L. Zhao and W. Yuan, Structure and Morphology of Thermoplastic Polyamide Elastomer Based on Long-Chain Polyamide 1212 and Renewable Poly(trimethylene glycol), *Ind. Eng. Chem. Res.*, 2020, **59**(39), 17502–17512, DOI: **10.1021/acs.iecr.0c01334**.

9 P. Kasprzyk, E. Głowińska, P. Parcheta-Szwindowska, K. Rohde and J. Datta, Green TPUs from Prepolymer Mixtures Designed by Controlling the Chemical Structure of Flexible Segments, *Int. J. Mol. Sci.*, 2021, **22**, 7438.

10 A. Petchsuk, W. Klinsukhon, D. Sirikittikul and C. Prahsarn, Parameters affecting transition temperatures of poly(lactic acid-co-polydiols) copolymer-based polyester urethanes and their shape memory behavior, *Polym. Adv. Technol.*, 2012, **23**(8), 1166–1173, DOI: **10.1002/pat.2017**.

11 L. Ugarte, A. Saralegi, R. Fernández, L. Martín, M. A. Corcuera and A. Eceiza, Flexible polyurethane foams based on 100% renewably sourced polyols, *Ind. Crops Prod.*, 2014, **62**, 545–551, DOI: **10.1016/j.indcrop.2014.09.028**.

12 Y.-S. Jung, S. Lee, J. Park and E.-J. Shin, One-Shot Synthesis of Thermoplastic Polyurethane Based on Bio-Polyol (Polytrimethylene Ether Glycol) and Characterization of Micro-Phase Separation, *Polymers*, 2022, **14**(20), 4269.

13 H. Wang, Y. Wang, C. Yuan, X. Xu, W. Zhou, Y. Huang, H. Lu, Y. Zheng, G. Luo, J. Shang, *et al.*, Polyethylene glycol (PEG)-associated immune responses triggered by clinically relevant lipid nanoparticles in rats, *npj Vaccines*, 2023, **8**(1), 169, DOI: **10.1038/s41541-023-00766-z**.

14 G. T. Kozma, T. Shimizu, T. Ishida and J. Szebeni, Anti-PEG antibodies: Properties, formation, testing and role in adverse immune reactions to PEGylated nano-biopharmaceuticals, *Adv. Drug Delivery Rev.*, 2020, **154–155**, 163–175, DOI: **10.1016/j.addr.2020.07.024**.

15 Y. Zhang, A. Y. Zhang, Z. G. Feng, L. Ye and R. X. Xu, Synthesis and characterization of polyether esters elastomer based on polyethylene glycol and poly(butylene terephthalate) - Influence of different hard segment length on polymer properties, *Acta Polym. Sin.*, 2002, (2), 167–172.

16 N. G. Khouri, J. O. Bahú, C. Blanco-Llamero, P. Severino, V. O. C. Concha and E. B. Souto, Polylactic acid (PLA): Properties, synthesis, and biomedical applications – A review of the literature, *J. Mol. Struct.*, 2024, **1309**, 138243, DOI: **10.1016/j.molstruc.2024.138243**.

17 K. Masutani and Y. Kimura, Chemistry, R. S., o. PLA Synthesis. From the Monomer to the Polymer, in *Poly(lactic acid) Science and Technology: Processing, Properties, Additives and Applications*, ed. A. Jiménez, M. Peltzer and R. Ruseckaite, The Royal Society of Chemistry, 2014.

18 M. Murariu and P. Dubois, PLA composites: From production to properties, *Adv. Drug Delivery Rev.*, 2016, **107**, 17–46, DOI: **10.1016/j.addr.2016.04.003**.

19 S. Saeidlou, M. A. Huneault, H. Li and C. B. Park, Poly(lactic acid) crystallization, *Prog. Polym. Sci.*, 2012, **37**(12), 1657–1677, DOI: **10.1016/j.progpolymsci.2012.07.005**.

20 A. J. Müller, M. Ávila, G. Ávila and J. Salazar, Chemistry, R. S., o. Crystallization of PLA-based Materials, in *Poly(lactic acid) Science and Technology: Processing, Properties, Additives and Applications*, ed. A. Jiménez, M. Peltzer and R. Ruseckaite, The Royal Society of Chemistry, 2014.

21 S. De Luca, D. Milanese, D. Gallichi-Nottiani, A. Cavazza and C. Sciancalepore, Poly(lactic acid) and Its Blends for Packaging Application: A Review, in *Clean Technologies*, 2023, vol. 5, pp. 1304–1343.

22 T. A. Swetha, A. Bora, K. Mohanrasu, P. Balaji, R. Raja, K. Ponnuchamy, G. Muthusamy and A. Arun, A comprehensive review on polylactic acid (PLA) – Synthesis, processing and application in food packaging, *Int. J. Biol. Macromol.*, 2023, **234**, 123715, DOI: **10.1016/j.ijbiomac.2023.123715**.

23 D. da Silva, M. Kaduri, M. Poley, O. Adir, N. Krinsky, J. Shainsky-Roitman and A. Schroeder, Biocompatibility, biodegradation and excretion of polylactic acid (PLA) in medical implants and theranostic systems, *Chem. Eng. J.*, 2018, **340**, 9–14, DOI: **10.1016/j.cej.2018.01.010**, from NLM.

24 J. S. Suk, Q. Xu, N. Kim, J. Hanes and L. M. Ensign, PEGylation as a strategy for improving nanoparticle-based drug and gene delivery, *Adv. Drug Delivery Rev.*, 2016, **99**, 28–51, DOI: **10.1016/j.addr.2015.09.012**.

25 D. Shi, D. Beasock, A. Fessler, J. Szebeni, J. Y. Ljubimova, K. A. Afonin and M. A. Dobrovolskaia, To PEGylate or not to PEGylate: Immunological properties of nanomedicine's most popular component, polyethylene glycol and its alternatives, *Adv. Drug Delivery Rev.*, 2022, **180**, 114079, DOI: **10.1016/j.addr.2021.114079**.

26 K. A. M. Thakur, R. T. Kean, E. S. Hall, J. J. Kolstad, T. A. Lindgren, M. A. Doscotch, J. I. Siepmann and E. J. Munson, High-Resolution 13C and 1H Solution NMR Study of Poly(lactide), *Macromolecules*, 1997, **30**(8), 2422–2428, DOI: **10.1021/ma9615967**.

27 Y. Ding, W. Feng, B. Lu, P. Wang, G. Wang and J. Ji, PLA-PEG-PLA tri-block copolymers: Effective compatibilizers for promotion of the interfacial structure and mechanical properties of PLA/PBAT blends, *Polymer*, 2018, **146**, 179–187, DOI: **10.1016/j.polymer.2018.05.037**.

28 J. Bao, X. Dong, S. Chen, W. Lu, X. Zhang and W. Chen, Confined crystallization, melting behavior and morphology in PEG-b-PLA diblock copolymers: Amorphous versus crystalline PLA, *J. Polym. Sci.*, 2020, **58**(3), 455–465, DOI: **10.1002/pol.20190077**.

29 O. Olabisi and L. M. Robeson, *Polymer-polymer miscibility*, Academic Press, 1979.

30 R. H. Staff, K. Landfester and D. Crespy, Recent Advances in the Emulsion Solvent Evaporation Technique for the Preparation of Nanoparticles and Nanocapsules, in *Hierarchical Macromolecular Structures: 60 Years after the Staudinger Nobel Prize II*, ed. V. Percec, Springer International Publishing, 2013, pp. 329–344.

31 E. Tinajero-Díaz, A. Martínez de Ilarduya and S. Muñoz-Guerra, Synthesis and properties of diblock copolymers of ω-pentadecalactone and α-amino acids, *Eur. Polym. J.*, 2019, **116**, 169–179, DOI: **10.1016/j.eurpolymj.2019.04.009**.

32 J. Panyam and V. Labhasetwar, Biodegradable nanoparticles for drug and gene delivery to cells and tissue, *Adv. Drug Delivery Rev.*, 2003, **55**(3), 329–347, DOI: **10.1016/S0169-409X(02)00228-4**.